AIChE

# Experimental Profiles of Lateral Mixing of Feed Particles in a Three-Dimensional Fluidized Bed

**Daoyin Liu and Xiaoping Chen**
School of Energy and Environment, Southeast University, Nanjing 210096, China

*DOI 10.1002/aic.12376*
*Published online August 16, 2010 in Wiley Online Library (wileyonlinelibrary.com).*

*Solids mixing data of high quality is one of the most crucial steps for quantitative studies, but it is a difficult task to obtain in a fluidized bed especially with a 3D configuration. Therefore a novel sampling technique is developed with bed collapse method, for measuring lateral mixing of feed particles in a 3D fluidized bed. The sampling tool is designed using a "bottom-to-top sampling" idea. Its development, configuration and measurement repetition are discussed in detail. The effects of mixing time, fluidizing gas velocity, and particle size of bed material on the tracer distribution are investigated. A quantitative comparison of lateral dispersion coefficient shows that our results agree fairly well with measurements and predictions of correlations for lab-scale fluidized systems in previous studies. The presented 2D profiles of the lateral mixing can be used to validate fundamental solids mixing models or verifying convenient measurement techniques.* © 2010 American Institute of Chemical Engineers *AIChE J,* 57: 1459–1469, 2011

*Keywords: fluidization, mixing, dispersion, tracer, bed collapse*

## Introduction

In fluidized bed combustors, lateral mixing of fuel particles fed into the bed influences distribution of the reacting particles and volatile gas over its cross section. If the mixing rate is smaller than that of the volatile release, the volatile distribution would be uneven.[1–4] Since it is important for design of fuel feed ports, there has been a continued interest in the lateral solids mixing in fluidized beds.[5] It is usually characterized by an effective dispersion coefficient, but the values are disconnected.[5] In the literature solids mixing in the lateral direction is less concerned than that in the axial direction which is studied more extensively characterized by residence time distribution.[6–8]

Correspondence concerning this article should be addressed to X. Chen at xpchen@seu.edu.cn.



Studies on solids mixing can be classified into two types mainly: interpretation of solids mixing mechanics, and estimation of mixing rate quantitatively. Various measurement techniques have been designed to elucidate solids mixing mechanics. A pulsed gas is injected into an incipient fluidizing bed composed of two layer particles in different colors, to observe mixing induced by a single bubble.[9–11] Positron emission particle tracking technique is employed to track a single particle trajectory continuously.[12] New developments have been also made for PEPT technique, such as Multiple-PEPT,[13] and positron emission tomography (PET).[14] Magnetic resonance tomography (MRT), a very expensive measurement technique, is applied to study small-scale fluidized systems with a very high spatial.[15] These studies, providing detailed information on bubble dynamic, particle trajectory, solids flow pattern, etc., do play an important role in knowledge of solids mixing mechanics in fluidized beds.

Through much efforts, qualitative mechanisms of solids mixing are well understood.[16,17] It is recognized that solid

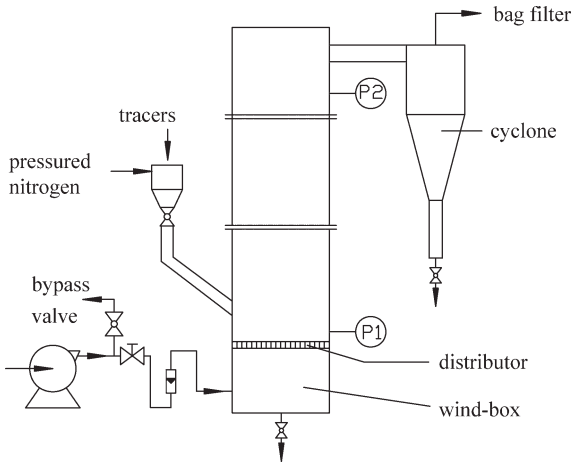


**Figure 1. Schematic diagram of fluidized bed apparatus.**

The bed has a rectangular cross section of 0.3 m × 0.2 m and a height of 2 m.

mixing is highly related with bubbles. As a bubble rises, it carries particles up in its wake and simultaneously pushes emulsion solids aside. The exchange of particles takes place between the ascending and descending emulsion solids. When it is close to the bed surface, the bubble bursts spreading the particles upon the bed surface. Some of the particles subsequently fall down and enter into the dense bed again, resulting in a gross circulation of solid phase. However, the solids mixing mechanisms are difficult to model or describe quantitatively.

Another type of studies on solids mixing is to estimate an overall solids mixing rate. A number of studies measured dispersion of a batch of tracers and fit the lateral mixing by a Fickian-type diffusion equation.[5] In this way, solids mixing induced by different factors, such as bubble movement and gross emulsion circulation, are lumped in an effective dispersion coefficient. However, the coefficient values are scattered in a broad range of 0.0001–0.1 $m^2/s$, resulting in scale up of solids mixing rate a challenging task.

Therefore, in the future, systematic experimental and theoretical investigations of solids mixing should be emphasized. The systematic experimental investigation, fundamental solids mixing model, or the combination of the both, can provide valuable tools.

As regards the experimental study, such a tracing technique that enables accurate, continuous, multipoints, and noncontaminated measurement, is still lacked for 3D fluidized beds. For instance, different chemical tracing method is not suitable for measuring tracers at several locations simultaneously[17,18]; thermal or dry ice tracing method contains uncertainties[3,19,20]; color tracing method is limited to 2D beds or countable number of bed particles[21]; PEPT or MRT are complex and expensive.[12,15] All these factors result that solids mixing data reported in the literature are not adequate. Efforts are still being made to develop new techniques to measure solids mixing.[22–25]

As regards the fundamental model, CFD simulation can provide insight into the behaviors of fluidized systems, such as Euler-Euler and Euler-Lagrangian models.[26,27] Nevertheless, it is a more challenging task for models to predict solids mixing than hydrodynamics only. Some authors reported Euler-Euler model over-predicted particle mixing.[28] And Euler-Lagrangian model is limited by its simulation scale of particle number. At present, the mechanics model of solids mixing is still lacked.[23]

After the above review, it seems that the quantitative investigations on solids mixing offer a challenge to both the experimental and theoretical investigations. It comes to our opinion that solids mixing data of high quality are precious, for verifying convenient measurement techniques or validating fundamental solids mixing models. Considering that most studies on lateral solids mixing only reported a single dispersion coefficient to represent the overall process, which is inadequate for validating solids mixing models, the present work is aimed to provide detailed and reliable experimental profiles of lateral solids mixing in a 3D fluidized bed.

In this work, we have developed a novel sampling technique with bed collapse method for measuring lateral mixing of feed particles in a 3D fluidized bed. A detailed description of the sampling method will be given and its robustness is discussed. The lateral mixing under different conditions of mixing time, fluidizing gas velocity and particle size are investigated. The results are compared quantitatively with previous works.

Compared with other tracing methods, the advantage of the developed method is reliable and cost effective, and it can be employed in 3D fluidized beds, but the disadvantage is laborious. Its limitation is that particle size of tracers should be different from that of bed material.

## Experimental

### *Apparatus*

Figure 1 shows the experimental system, consisting of a gas supply unit, a 3D fluidized bed, and tracer injection and detection components. The fluidized bed riser, with a rectangular cross section of 0.3 m × 0.2 m and a height of 2 m, has a gas distributor with 24 bubble caps and 4.7% open fraction. A cyclone is installed at the riser exit to capture fine particles carried away by the fluidizing gas. The lower part of the front side of the riser is made of transparent Perspex, which enables camera recording of fluidization patterns. A window is made on the back side of the riser to put in/out a sampling tool. A butterfly valve is installed at the gas supply line to cut off the fluidizing air rapidly.

### *Materials*

The bed material composes of 6600 g sand particles. Sand is screened in three narrow particle size ranges. Table 1 lists the particle density, particle size range, and minimum fluidization velocity ($U_{mf}$) determined by experiments. Sand particles with the same density, but larger particle size of 0.8–1.0 mm, are used as tracers. In each run, the mass of tracers

**Table 1. Particle Properties of Bed Materials**

| Material | $d_p$ (mm) | $\rho_p$ (kg/m$^3$) | $U_{mf}$ (m/s) |
|---|---|---|---|
| Sand | 0.22–0.28 | 2600 | 0.08 |
| Sand | 0.28–0.45 | 2600 | 0.19 |
| Sand | 0.45–0.60 | 2600 | 0.41 |

$U_{mf}$ was determined by experiments.

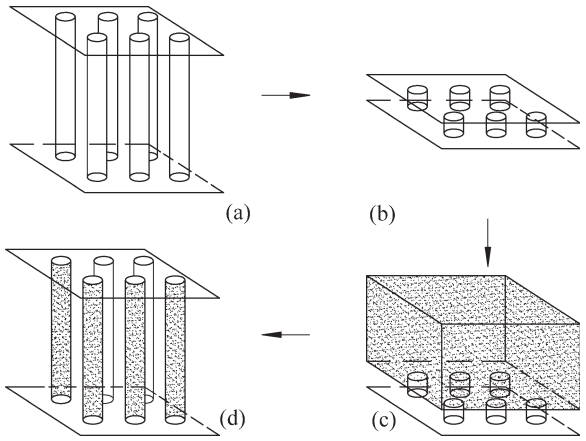


**Figure 2. Schematic principle of the sampling tool.**

is 1370 g. The mass of bed material and tracers are maintained constant in differential experimental runs.

### *Tracer injection*

A tracer container with a feed tube is located at the sidewall of the riser, shown in Figure 1. The feed tube, with an inner diameter of 38 mm, connects the riser with an angle of 40 degree at a height of 0.15 m above the distributor. A ball valve is installed in the feed tube. In each run, when the bed has reached steady-state fluidization, a batch of weighed tracers is poured into the container. Then at one moment, the valve is opened quickly and the tracers flow into the bed. At the same time, timing is started. After a specified interval, i.e., 5, 10, 30 s, the fluidizing gas is cut off quickly and the bypass valve opened simultaneously, resulting in the bed material collapsing. It should be mentioned that the tracers can flow into the bed solely by the gravity, because the feed port is located in the splashed zone. There is also a flow of pressured $N_2$ connected to the tracer container. By adjusting the flow rate of the pressured $N_2$, it can, to some extent, facilitate or accelerate the tracers flowing into the bed.

### *Tracer detection*

A novel sampling tool is designed to measure the lateral distribution of tracers. Figure 2 shows its principle, as the sequence from (a) to (b). It is made up of two plates and 24 sleeves, with the two plates joining the sleeves together, as shown in Figure 2a. Before each run, the 24 sleeves are folded, and the two plates pressed together with the bottom one fixed at the gas distributor, Figure 2b. The sampling tool is designed to fit the layout of the 24 bubble caps and the orifices on the bubble caps are above the upper plate when the sampling tool is folded. Thus, the sampling tool does not disturb the gas distributing.

After the sampling tool is folded, a batch of weighed bed material is poured into the bed, with the sampling tool below the bed material, Figure 2c.

After the above preparations, the air blower is turned on and the gas flow rate is adjusted according to a desired operating condition. The bed is fluidized for a while to reach steady-state fluidization. Then injection of the tracers and "freezing" the bed are followed as described in the section of "Tracer injection."

After the bed collapses, the window on the back side of the bed is opened. The upper plate of the sampling tool is brought up very slowly by pulling up wire ropes connecting with it. As the upper plate is going up, the sleeves are unfolded which induces the particles to flow into their nearby sleeves accordingly. As a result, 24 samples are obtained, Figure 2d. The top view and index of the samples are shown in Figure 3. Then particles in each sample cell are sucked by an electric vacuum cleaner, separated by screening, and weighed. In each sample cell, the mass of bed material and tracers are marked as $m_0$ and $m_1$, and the local tracer concentration ($\eta$) is defined as the ratio of $m_0$ over the sum of $m_0$ and $m_1$.

The sampling tool is designed according to a novel idea: sampling from bottom to up. It has several advantages. When sampling horizontally, the resistance between the sampling tool and particles is large, which could alter the lateral positions of the particles. In the early stages of the experiments, we also tried sampling from top to bottom. Unfortunately, the sampling tool could not be inserted into the bed material easily. The resistance became much larger as the sampling tool was pressed down further, leading the sampling depth was less than 2 cm. Besides, the particles could be crushed in this way. However, the tool designed with the "bottom-to-up sampling" idea has been proved to have good performance. Since the particles can flow automatically into the cells by the gravity during sampling, the resistance is so small that particles can be collected easily. A particular advantage is that there are constantly enough particles in each sample cell, which enables the sample a good representation of the bed mixing.

## Preliminary Evaluations

During the processes of injection, detection, and separation of tracer particles, uncertainties may exist. For instance, maybe the injection velocity influences subsequent mixing; the tracers are attrited during fluidization and screen. Moreover, due to the fact that the motion of a single particle is quite random, are the measured distribution of tracers at a "frozen" bed representative or repeatable? These uncertainties are checked first.

To reflect the process of tracer injection and bed collapse, the pressure drop between two points of P1 and P2 in Figure 1 is monitored by a pressure drop sensor. Figure 4 shows the pressure drop response in a typical test ($d_p$ = 0.28–0.45 mm,

| | | | | | | |
|---|---|---|---|---|---|---|
| Row 4 | 24 | 23 | 22 | 21 | 20 | 19 |
| Row 3 | 18 | 17 | 16 | 15 | 14 | 13 |
| Row 2 | 12 | 11 | 10 | 9 | 8 | 7 |
| Row 1 | 6 | 5 | 4 | 3 | 2 | 1 |

feed port

y

x

**Figure 3. Top view and index of sample cells.**

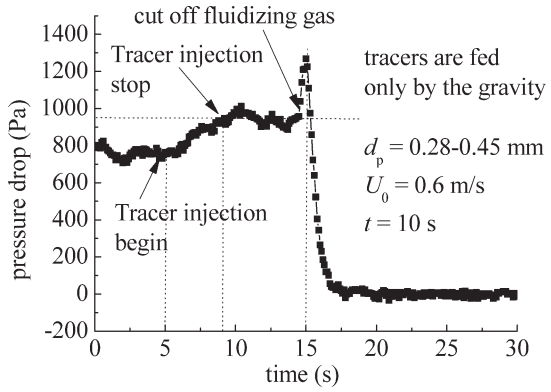


**Figure 4. Pressure drop response in a typical test ($d_p$ = 0.28–0.45 mm, $U_0$ = 0.6 m/s, $t$ = 10 s) due to tracer injection and bed collapse.**

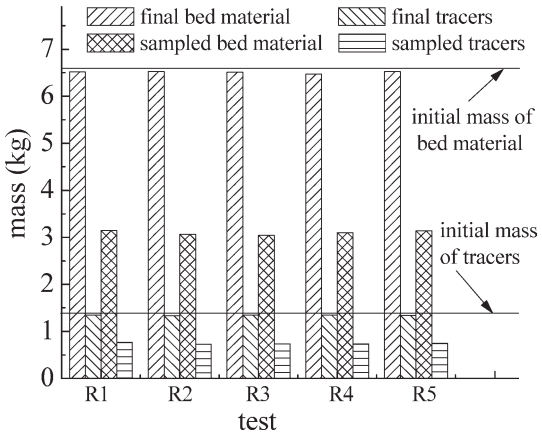


**Figure 5. Illustration of balance of initial mass, sampled mass, and final mass for bed material and tracers.**

Five repeated tests, R1–R5, on the condition ($d_p$ = 0.28–0.45 mm, $U_0$ = 1.2 m/s, $t$ = 10 s) are shown for example.

$U_0$ = 0.6 m/s, $t$ = 10 s), in which the tracers are fed only by the gravity. The pressure drop trace is started at $t$ = 0 s, and at $t$ = 5 s it begins to increase because a batch of tracers begins feeding into the bed, and at round $t$ = 9 s it reaches a steady-sate value indicating the tracer feeding is completed. At $t$ = 15 s the pressure drop rises shortly and falls down to zero, because the fluidizing gas is cut off rapidly. From the response of the pressure drop, it can be read that the feeding duration is about 4 s. Given the feeding duration and total mass of tracers, the feeding velocity of tracers is calculated to be 0.11 m/s.

During experiments it is found that the feeding duration is always around 4 s as the tracers are fed only by the gravity. If the pressured $N_2$ is turned on at 4 $m^3$/h and 0.2 MPa, the feeding duration can be reduced to be around 2.5 s. Accordingly, the tracer particle velocity is increased to 0.19 m/s. In the preliminary tests, experiments with different tracer particle velocity from 0.11 m/s to 0.19 m/s are compared, but we can not observe noticeable difference of lateral distribution of tracer concentration between these tests. It indicates that the mixing of feed particles mainly depends on fluidized bed dynamics, because the tracers quickly lose their momentum and are dispersed by the bed material when they are fed at a low velocity. Therefore, for all the tests listed in Table 2 the tracers are fed only by the gravity.

The mass balance of the particles before tracing and after sampling is checked for each run. In each run, the initial mass of bed material and tracers are constant. The mass of bed material and tracers collected in the 24 sample cells, are summed up as sampled mass. There remain some bed materials and tracers in the bed after sampling. The mass of the remained particles is added to the sampled mass, yielding the final mass. The balance of initial mass, sampled mass, and final mass for five repeated tests on the condition ($d_p$ = 0.28–0.45 mm, $U_0$ = 1.2 m/s, $t$ = 10 s) are presented in Figure 5. Experiments show that, in different tests, the final mass is almost equal to the initial mass of the bed material or tracers, indicating attrition during experiments is negligible. Also, the sampled mass always shared ~50% of the initial mass, ensuring the samples a good representation of the bed mixing.

**Table 2. Test Conditions**

| Set | $d_p$ (mm) | $U_0$ (m/s) | $t$ (s) |
|---|---|---|---|
| S1 | 0.22–0.28 | 0.6 | 10 |
| S2 | 0.22–0.28 | 1.2 | 10 |
| M1 | 0.28–0.45 | 0.6 | 5, 10, 15, 20, 30 |
| M2 | 0.28–0.45 | 1.2 | 5, 10, 15, 20, 30 |
| M3 | 0.28–0.45 | 1.7 | 10 |
| M4 | 0.28–0.45 | 2.3 | 10 |
| L1 | 0.45–0.60 | 0.8 | 10 |
| L2 | 0.45–0.60 | 1.2 | 10 |
| L3 | 0.45–0.60 | 1.7 | 10 |
| L4 | 0.45–0.60 | 2.3 | 10 |

To investigate whether the measured tracer concentrations at one mixing time are representative, five runs are repeated for a test condition ($d_p$ = 0.28–0.45 mm, $U_0$ = 1.2 m/s, $t$ = 10 s). Figure 6a presents the lateral tracer concentration profiles ($\eta$) for one of the five repeats, and Figure 6b the averaged $\eta$ with error bar for the five repeats. It can be seen that the measurements on dispersion of a batch of particles is well repeatable and the maximal error is below 3%. Therefore, the dispersion of a batch of tracers is measurable, and the measurements are repeatable not only qualitatively but also quantitatively.

## Results and Discussion

Several levels of fluidizing gas velocity ($U_0$) and mixing time ($t$) are investigated for each bed material ($d_p$) listed in Table 1. Their combinations are given in Table 2. In a test, the mass of the bed material and tracers in each of the 24 sample cells are recorded, yielding a lateral distribution of tracer concentration ($\eta$). The complete set of the lateral distribution of $\eta$ is reported in an Appendix table.

### *Mixing process with time*

Figure 7 illustrates the lateral mixing process of tracers at $t$ = 5, 15, and 30 s, with bed material particle size ($d_p$) of 0.28–0.45 mm and fluidizing gas velocity ($U_0$) of 0.6 m/s. Each instantaneous distribution shows that the local tracer concentration decreases with the distance from the tracer source. As time proceeds, the concentrations at different

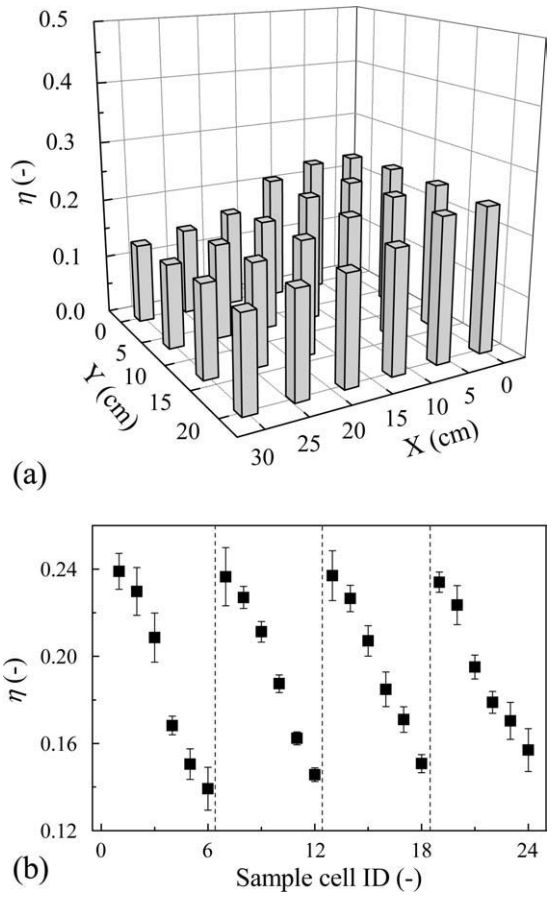


**Figure 6. (a): Lateral tracer concentration profiles for five repeats at the condition ($d_p$ = 0.28–0.45 mm, $U_0$ = 1.2 m/s, $t$ = 10 s); (b): Averaged values with error bar of the tracer concentrations for the five repeats.**

positions are leveled off, indicating the tracers are gradually dispersed from the feed port.

Figure 8 illustrates the lateral mixing process at $t$ = 5, 15, and 30 s, under the condition of $d_p$ = 0.28–0.45 mm and $U_0$ = 1.2 m/s. With $U_0$ increased from 0.6 m/s to 1.2 m/s, the tracer concentration differences at different sample cells become smaller, but the evolvement of the tracer concentration distribution for both the conditions are similar. The results presented in Figures 7 and 8 are self-explanation that the feed particles are gradually dispersed from the tracer source with time. Usually, the lateral mixing is fitted by a Fickian-type diffusion equation.[5,16]

### *Mixing under different conditions*

Examples of the tracer concentration profiles at the conditions of different gas velocity and particle size are presented in (i) Figure 9a for bed material composed of $d_p$ = 0.22–0.28 mm sand, (ii) Figure 9b for $d_p$ = 0.28–0.45 mm, (iii) and Figure 9c for $d_p$ = 0.45–0.60 mm. The samples form No. 1 to 6 are plotted. Each figure shows the effect of fluidizing velocity on the tracer concentration profile, with constant particle size and mixing time.

It is clear from Figure 9 that the tracer concentration distribution becomes more even with increase in fluidizing gas velocity. It is a consistent conclusion that fluidizing gas velocity has an active influence on solids mixing. As $U_0$ is increased, the bubble dynamics become more intense which promote solids mixing.

In Figure 10, $U_0$ is plotted as a parameter and $d_p$ as a variable. It shows the effect of $d_p$ on the tracer concentration profile with $U_0$ = 1.2 m/s. The mixing under the condition of $d_p$ = 0.22–0.28 mm is better than the other two conditions. This finding is useful in practice: in fluidized bed combustors, while the flow rate of fluidizing air is determined by fuel consumption, it is feasible to improve solids mixing by controlling the bed material with a distribution of smaller particle size.

The complete set of the lateral distribution of tracer concentration under different conditions of gas velocity and particle size is listed in an Appendix table. As reviewed in the Introduction section, solids mixing data of high quality are precious for validating solids mixing models, whereas a single dispersion coefficient representing the overall mixing process is inadequate for validating solids mixing models. The reported 2D profiles of the tracer concentration can be used to validate solids mixing models or verify other convenient measurement techniques.

### *Lateral dispersion coefficient*

A number of studies reported the values of effective dispersion coefficient in fluidized beds.[5] For comparison with their measurements, the dispersion coefficient is calculated

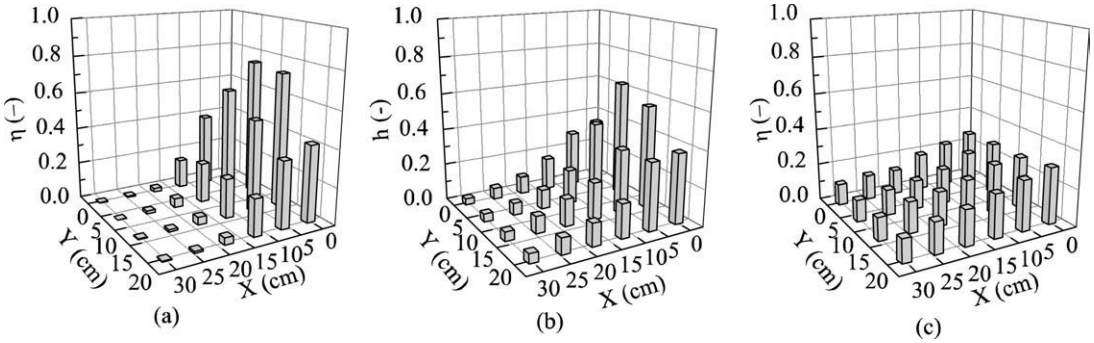


**Figure 7. Lateral tracer concentration profiles measured at $t$ = 5, 15, and 30 s, with $d_p$ = 0.28–0.45 mm and $U_0$ = 0.6 m/s.**

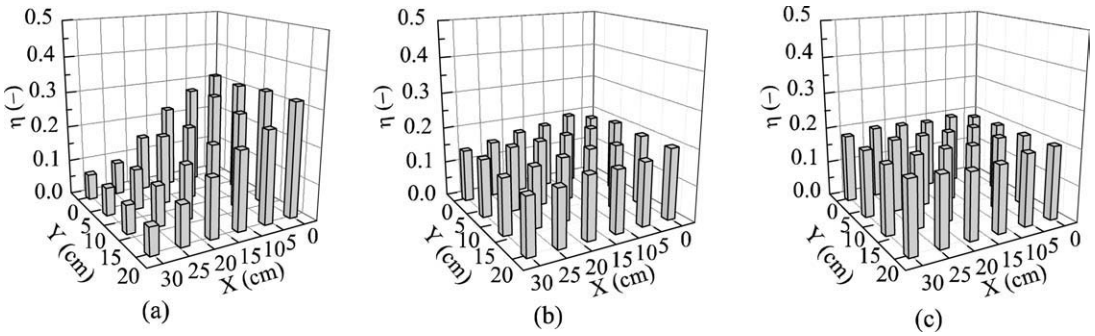


**Figure 8. Lateral tracer concentration profiles measured at $t$ = 5, 15, and 30 s, with $d_p$ = 0.28–0.45 mm and $U_0$ = 1.2 m/s.**

here. For a 3D fluidized bed in this study, the lateral mixing can be described by a 2D Fickian-type diffusion equation,

$$\frac{\partial C}{\partial t} = \frac{\partial}{\partial x}\left(D_{sr}\frac{\partial C}{\partial x}\right) + \frac{\partial}{\partial y}\left(D_{sr}\frac{\partial C}{\partial y}\right) + S_{feed} \qquad (1)$$

where $C$ is tracer mass concentration per cross-section area (kg/m$^2$), $S_{feed}$ tracer source (kg/m$^2$s) determined by the experimental condition, and $D_{sr}$ effective lateral solids dispersion coefficient (m$^2$/s) which lumps together convective and diffusion terms.

Equation 1 is solved with proper initial and boundary conditions. If the initial condition is set by concentrations measured at 5 s, $S_{feed}$ is zero and the boundary condition $\partial C/\delta x = 0$, $\partial C/\delta y = 0$. If the initial condition is set by zero, $S_{feed}$ is calculated as $S_{feed}$ = tracer mass/duration of feeding tracers/initial spread area of tracers. While the tracer mass and duration of feeding tracers are determined, the initial spread area has to be assumed. An assumption is 4 cm × 5 cm around the feed point. During the preprimary calculation, the sensitivity of the initial spread area on the prediction of tracer distribution is checked. It is found there is no evident difference of predictions as the initial spread area is changed within a reasonable range.

The solution of Eq. 1 is a distribution of tracer mass concentration per cross-section area. It is first converted to a distribution of tracer mass fraction, $\eta$, and then compared with measurements. Different values of $D_{sr}$ are selected for Eq. 1, until the error between the prediction and measurement is small enough.

Figure 11 shows the evolvement of tracer concentration profiles, predicted by Eq. 1 with $D_{sr}$ = 0.0005 m$^2$/s. Also, the concentrations at sample cells from No. 7 to 12 are extracted and compared with measurements at $d_p$ = 0.28–0.45 mm and $U_0$ = 0.6 m/s. With $D_{sr}$ = 0.0005 m$^2$/s, Eq. 1 matches the measured concentrations mostly. Although the predicted and measured concentrations do not agree well near the bed wall at $t$ = 10, 15, and 20 s, their difference disappears almost at $t$ = 30 s.

An alternative method for matching the predicted and measured concentrations is to assume a distribution of $D_{sr}$, not a single value. Figure 12 illustrates the distribution of $D_{sr}$ over the cross section, the predicted tracer concentration profiles accordingly, and their comparisons with the measurement, for the condition considered in Figure 11. To match the prediction and measurement, the values of $D_{sr}$ near the bed wall at $t$ = 10 s have to be assumed very small. As time proceeds, the difference of $D_{sr}$ near the bed wall and in the core region decreases. At $t$ = 30 s, a uniform distribution of $D_{sr}$ enables the predicted concentrations match the measured ones. The above uneven distribution of $D_{sr}$ inferred from the measurement at a very short time interval, indicates solids mixing is faster in the core region than the wall region, which agrees with the flow structure in fluidized beds: bubble dynamics are more intense in the core region. Given sufficient time for mixing, $D_{sr}$ is predicted to be uniform, because the tracers move around in the core region and near the bed wall.

Since a single value of $D_{sr}$ is acceptable to match the predicted and measured tracer concentration profiles generally,

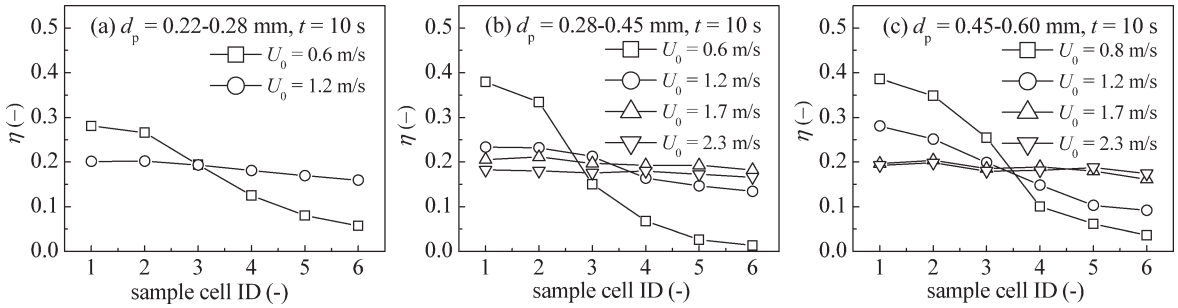


**Figure 9. Effect of $U_0$ on tracer concentration distribution at $t$ = 10 s for three bed materials: (a) $d_p$ = 0.22–0.28 mm; (b) $d_p$ = 0.28–0.45 mm; (c) $d_p$ = 0.45–0.60 mm.**

Sample cells from No. 1 to 6 are plotted.

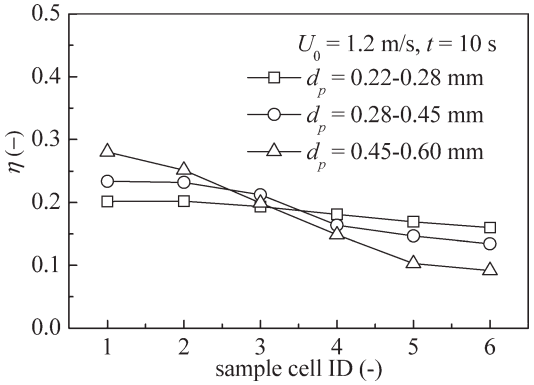


**Figure 10. Effect of $d_p$ on tracer concentration distribution at $t$ = 10 s with $U_0$ = 1.2 m/s.**

Sample cells from No. 1 to 6 are plotted.

Eq. 1 with a const value of $D_{sr}$ is solved to match measurements for conditions covering the range of two levels of fluidizing gas velocity for each of the three bed materials. Their comparisons are shown in Figure 13. In each plot the test index and a proper value of $D_{sr}$ are indicated. The reported values of $D_{sr}$ lie in the range of 0.0005–0.0035 $m^2/s$.

### *Compared with existing correlation and values*

A number of works reported the values of $D_{sr}$ in dense fluidized beds and several correlations were also proposed.[5,24] Table 3 lists the correlations of $D_{sr}$ published in journals. It should be noted that Eq. 2 can be only applicable for fast bubbles which satisfies $u_{bub,r} > 2u_{mf}/\varepsilon_{mf}$. Figure 14 compares their predictions with the results exacted from Figure 13. The $D_{sr}$ is plotted as a function of $U_0 - U_{mf}$. The agreement between the predictions and our measured data are good, expect that the measurements in the present work are somewhat smaller than the predictions. A possible reason is that in the present work the tracers are larger than that of the bed materials.

Since Niklasson et al.[5] made an exhaustive list of measurements on $D_{sr}$ with the corresponding experimental conditions, such a summarized list is not repeated here. From Figure 2 or Table 1 of the paper by Niklasson et al.,[5] we note that while the values of $D_{sr}$ are scattered in a broad range of 0.0001–0.1 $m^2/s$, most of them lie in a smaller range of 0.0002–0.0050 $m^2/s$. The range of $D_{sr}$ in several works agrees with our measurements: Berruti et al.,[18] Bellgardt and Werther,[19] Salam et al.,[30] and Bi et al.[31] measured $D_{sr}$ to be around 0.0002–0.0020, 0.0007–0.0026, 0.0005–0.0020, and 0.0004–0.0016 $m^2/s$, respectively. But $D_{sr}$ measured by Shi and Fan,[17] and Winaya et al.[24] are smaller, being around 0.0001–0.0008 and 0.0004 $m^2/s$, respectively, probably because their experiments were conducted in 2D fluidized beds with very small thickness where bubble dynamics were oppressed. Besides, a few works conducted in wider facilities under high fluidizing velocities reported $D_{sr}$ to be around (or larger than) 0.01 $m^2/s$. From industrial application or scale-up view, these measurements are more valuable, but the number of reports in this range is much fewer. The above comparisons indicate that $D_{sr}$ depends not only on particle and fluidizing gas properties but also on the size of fluidized beds. The further reason for the effect of bed size on $D_{sr}$ is left open here, because the measurements obtained in wider fluidized beds are not sufficient. Probably a validated fundamental solids mixing model can be helpful to investigate this question.

### *Compared with thermal tracing method*

The tracer concentration profiles presented above can be used to validate solids mixing models or verify convenient measurement techniques. To give an example of the application, the above mixing data are used to verify measurement from the thermal tracing method. Thermal tracing method can investigate solids mixing behaviors on-line, and the heated/cooled tracers do not contaminate bed material. But the disadvantage is uncertainties for inferring the local tracer concentration from the temperature measurements.[3] Here the thermal tracing measurement is compared with the reliable measurements preliminarily.

When the bed has reached steady-state fluidization, a batch of 100C tracers is fed into the bed. All the operating

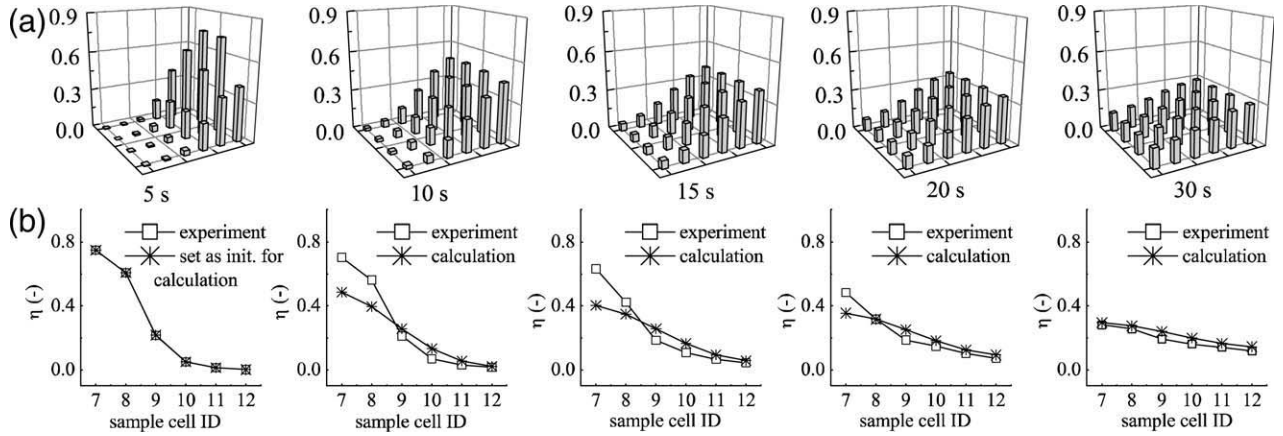


**Figure 11. A single value of $D_{sr}$ for matching the predicted and measured tracer concentration profiles.**

(a) 1st Row, evolvement of tracer concentration profiles predicted with $D_{sr}$ = 0.0005 $m^2/s$, the initial condition set by concentrations measured at 5 s; (b) 2nd Row, comparisons of prediction and measurements at $d_p$ = 0.28–0.45 mm and $U_0$ = 0.6 m/s. Comparisons of sample cells from No. 7 to 12 are shown.

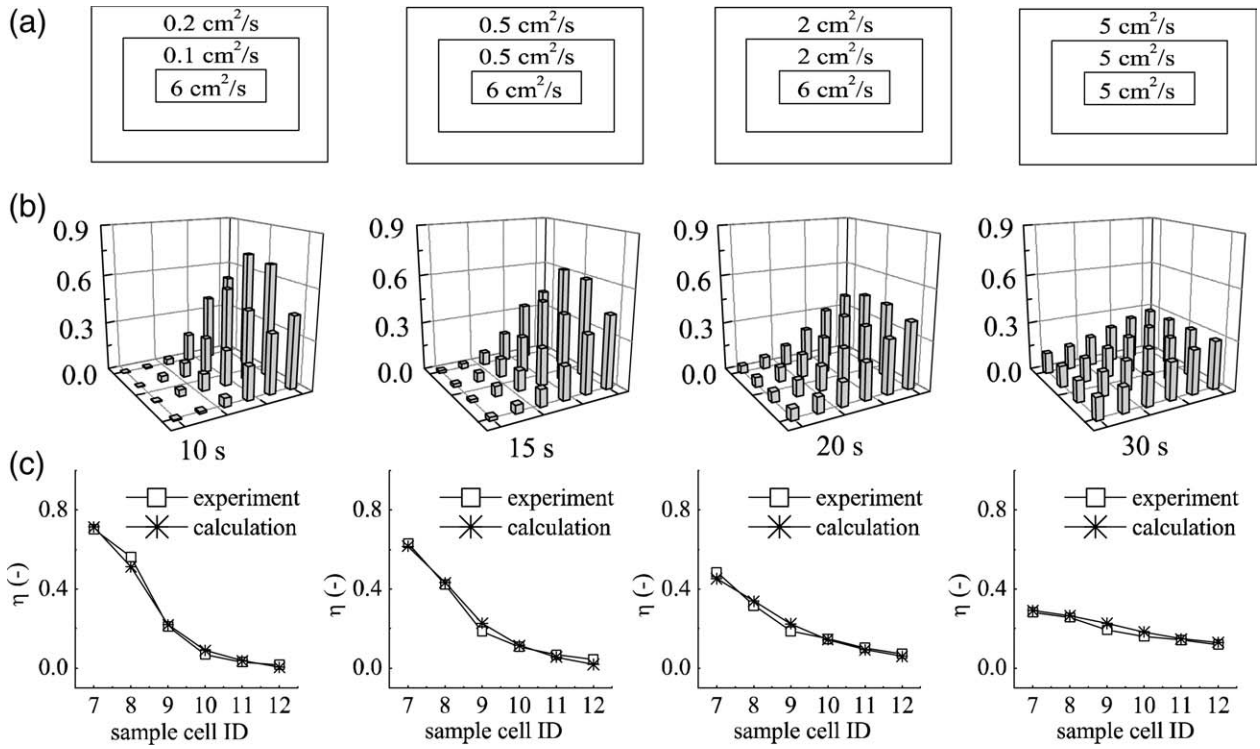


**Figure 12. A distribution of $D_{sr}$ for matching the predicted and measured tracer concentration profiles.**

(a) 1st Row, distribution of $D_{sr}$; (b) 2nd Row, evolvement of tracer concentration profiles predicted with the corresponding $D_{sr}$, the initial condition set by concentrations measured at 5 s; (c) 3rd Row, comparisons of prediction and measurements at $d_p$ = 0.28–0.45 mm and $U_0$ = 0.6 m/s. Comparisons of sample cells from No. 7 to 12 are shown.

parameters including particle size of the tracers, are kept the same as test M2 ($d_p$ = 0.28–0.45 mm and $U_0$ = 1.2 m/s). Twenty-four thermistors are located at positions according to sample cells illustrated in Figure 3, at a same height of 0.12 m above the gas distributor.

Figure 15 presents the transient temperatures at monitor probes from No. 1 to 12. The temperature rise depends on the distance of the monitor probe from the feed port. The largest temperature rise is found for No. 1 and 7 which are nearest from the feed port. The smaller temperature rise is found for probes further from the feed port. For comparison, a zoom-in view of Figure 15a is presented in Figure 16a. And the tracer concentration in Figure 8 is rearranged in Figure 16b: by plotting the tracer concentration against time with sample cell ID as a parameter. It is noted that the trend of the transient changes presented in the Figures 16a, b are very similar, while the heat tracing measurements are somewhat delayed by several seconds. It

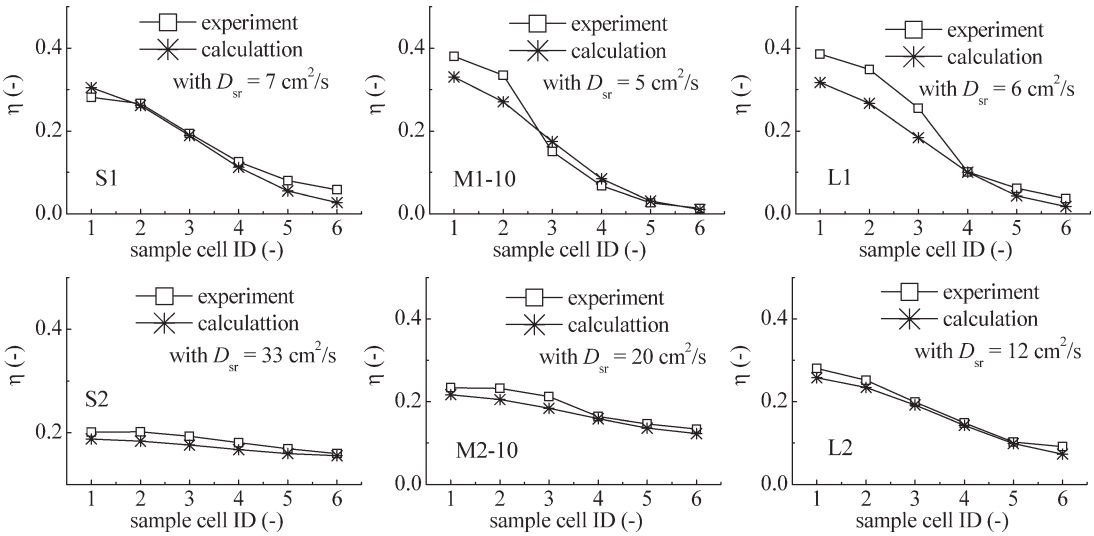


**Figure 13. Comparisons of measurements and prediction with $D_{sr}$.**

Each plot reports a proper value of $D_{sr}$, with experimental run index indicated.

**Table 3. Correlations of Lateral Solids Dispersion Coefficient**

| References | Correlations | |
|---|---|---|
| 16 | $D_{sr} = \frac{3}{16}\frac{\delta}{1-\delta}\alpha^2 d_{bub} u_{bub,r}\left(\left(\frac{u_{bub,r}+2u_{mf}/\varepsilon_{mf}}{u_{bub,r}-2u_{mf}/\varepsilon_{mf}}\right)^{1/3}-1\right)$ | Eq. 2 |
| 29 | $D_{sr} = 0.013(u_0 - u_{mf})h_0\left(\frac{D_{bed}}{h_0}\right)^{0.5}\left(\frac{(u_0-u_{mf})^2}{gh_0}\right)^{-0.15}$ | Eq. 3 |
| 17 | $D_{sr} = 0.46(u_0 - u_{mf})h_0\left(\frac{(u_0-u_{mf})d_p\rho_g}{\mu_g}\right)^{-0.21}\left(\frac{h_0}{d_p}\right)^{0.24}\left(\frac{\rho_p-\rho_g}{\rho_g}\right)^{-0.43}$ | Eq. 4 |
| 18 | $D_{sr} = 0.185\left(1-(0.44+2.87h/h_0)(r/R)^5\right)$ $(u_0 - u_{mf})d_p\left(\frac{(u_0 - u_{mf})d_p\rho_g}{\mu_g}\right)^{-0.25}\left(\frac{h_0}{d_p}\right)^{1.45}\left(\frac{\rho_p - \rho_g}{\rho_g}\right)^{-0.43}$ | Eq. 5 |
| 19 | $D_{sr} = 0.00067 + 0.023\frac{1}{H}\int_0^H \frac{\delta}{1-\delta}\sqrt{gd_{bub}^3}dh$ | Eq. 6 |

demonstrates that the result from the thermal tracing method is helpful to estimate the solids mixing rate. The detailed/quantitative interpretation for the temperature measurements should consider the couple effects of the mixing and heat transfer, which is being conducted in the ongoing work.

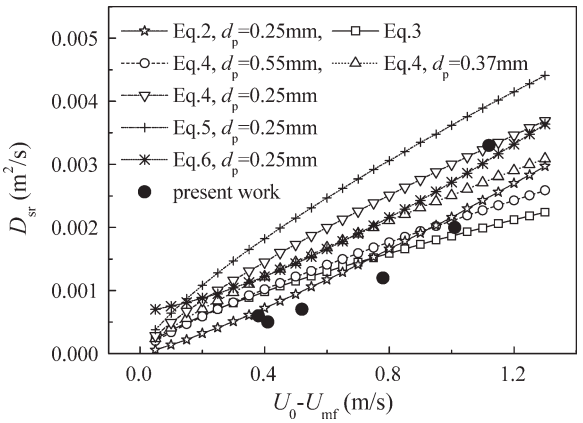


**Figure 14. Comparisons of $D_{sr}$ with predictions by correlations.**

## Conclusions

A brief review of solids mixing in fluidized beds shows that quantitative investigations should be emphasized in the future studies, but the quantitative investigations offer a challenge to both the experimental and theoretical investigations. The reliable and detailed solids mixing data would be precious in quantitative investigations.

A novel sampling technique is developed applied with bed collapse method to obtain reliable lateral mixing profiles of feed particles in a 3D fluidized bed. The sampling tool is designed using a ''bottom-to-top sampling'' idea. An extensive set of measurements on the distribution of tracer particles are carried out for different mixing time, fluidizing gas velocity and particle size.

A quantitative comparison of lateral solids dispersion coefficient shows that it is greatly influenced by the size of fluidized beds. Our results agree fairly well with the measurements and predictions of correlations for lab-scale fluidized systems by previous studies.

The reported 2D profiles of the tracer concentration can be used to validate solids mixing models or verify other convenient measurement techniques. A preliminary validation of thermal tracing method is given.

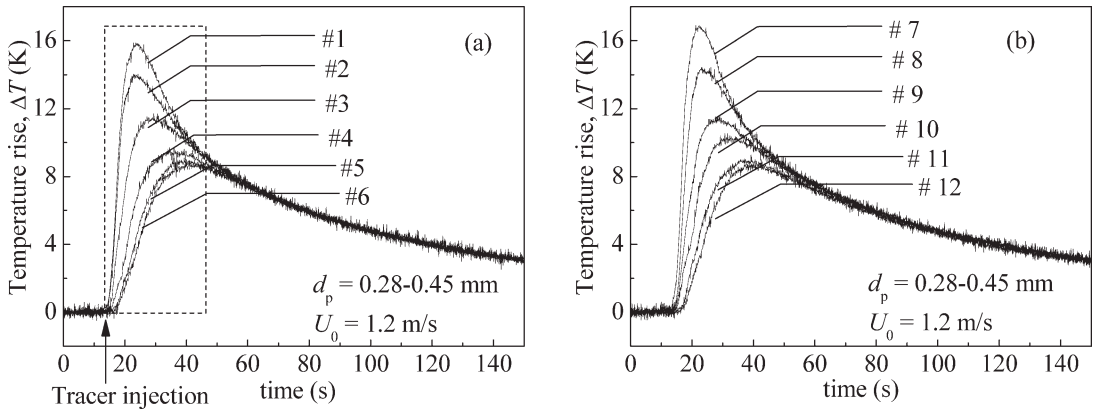


**Figure 15. Transient temperature profiles due to a pulsed feeding of heated particles at $d_p$ = 0.28–0.45 mm and $U_0$ = 1.2 m/s.**

(a) Monitor points from No. 1 to 6; (b) monitor points from No. 7 to 12.

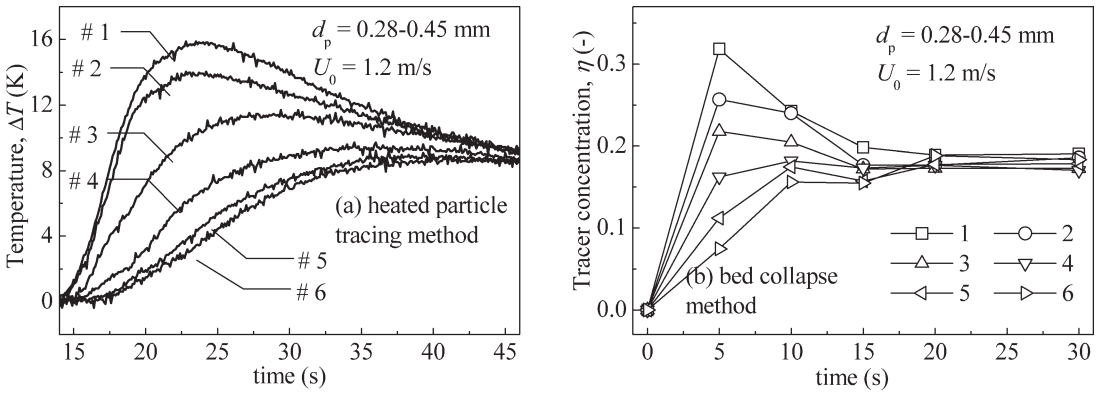


**Figure 16. Comparisons of measurements from two tracing methods at $d_p$ = 0.28–0.45 mm and $U_0$ = 1.2 m/s.**

(a) Transient temperature profiles from No. 1 to 6 (a zoomed-in view from Figure 15a); (b) transient tracer concentration profiles at sample cells from No. 1 to 6 (by plotting tracer concentration presented in Figure 8 against time with sample cell ID as a parameter).

## Acknowledgments

Financial support of this work provided by National Key Technology R&D Program (2006BAA03B02-10), the High-tech Research and Development Program of China (2009AA05Z311), and the Scientific Research Foundation of Graduate School of Southeast University is gratefully acknowledged. The authors thank anonymous Reviewers of this article for their insightful and detailed comments which helped to improve it significantly.

## Literature Cited

1. Leckner B. Fluidized bed combustion: mixing and pollutant limitation. *Prog Energy Combust Sci.* 1998;24:31–61.
2. Hartge EU, Luecke K, Werther J. The role of mixing in the performance of CFB reactors. *Chem Eng Sci.* 1999;54:5393–5407.
3. Glicksman L, Carr E, Noymer P. Particle injection and mixing experiments in a one-quarter scale model bubbling fluidized bed. *Powder Technol.* 2008;180:284–288.
4. Pallarès D, Johnsson F. Modeling of fuel mixing in fluidized bed combustors. *Chem Eng Sci.* 2008;63:5663–5671.
5. Niklasson F, Thunman H, Johnsson F, Leckner B. Estimation of solids mixing in a fluidized-bed combustor. *Ind Eng Chem Res.* 2002;41:4663–4673.
6. Du B, Fan LS, Wei F, Warsito W. Gas and solids mixing in a turbulent fluidized bed. *AIChE J.* 2002;48:1896–1909.
7. Harris AT, Davidson JF, Thorpe RB. Particle residence time distributions in circulating fluidised beds. *Chem Eng Sci.* 2003;58:2181–2202.
8. Werther J, Hirschberg B. *Solids motion and mixing*. In: Grace JR, Avidan AA, Knowlton T, editors. *Circulating Fluidized Beds*. London: Blackie Academic & Professional, 1996:119–148.
9. Rowe P, Partridge B, Cheney A, Henwood G. The mechanics of solids mixing in fluidised beds. *Trans Inst Chem Eng.* 1965;43:271–286.
10. Woollard NM, Potter OE. Solids mixing in fluidized beds. *AIChE J.* 1968;14:388–391.
11. Eames I, Gilbertson MA. Mixing and drift in gas-fluidised beds. *Powder Technol.* 2005;154:185–193.
12. Stein M, Ding YL, Seville JPK, Parker DJ. Solids motion in bubbling gas fluidised beds. *Chem Eng Sci.* 2000;55:5291–5300.
13. Yang Z, Fan X, Bakalis S, Parker DJ, Fryer PJ. A method for characterising solids translational and rotational motions using multiple-positron emission particle tracking (Multiple-PEPT). *Int J Multiphase Flow.* 2008;34:1152–1160.
14. Dechsiri C, Van der Zwan EA, Dehling HG, Hoffmann AC. Dispersion of particle pulses in fluidized beds measured by positron emission tomography. *AIChE J.* 2005;51:791–801.
15. Müller CR, Holland DJ, Sederman AJ, Mantle MD, Gladden LF, Davidson JF. Magnetic resonance imaging of fluidized beds. *Powder Technol.* 2008;183:53–62.
16. Kunii D, Levenspiel O. *Fluidization Engineering*, *2nd ed.* Boston: Butterworth-Heinemann Press, 1991.
17. Shi YF, Fan LT. Lateral mixing of solids in batch gas-solids fluidized beds. *Ind Eng Chem Process Des Dev.* 1984;23:337–341.
18. Berruti F, Scott DS, Rhodes E. Measuring and modelling lateral solid mixing in a three-dimensional batch gas-solid fluidized bed reactor. *Can J Chem Eng.* 1986,64:48–56.
19. Bellgardt D, Werther J. A novel method for the investigation of particle mixing in gas-solid systems. *Powder Technol.* 1986;48:173–180.
20. Schlichthaerle P, Werther J. Solids mixing in the bottom zone of a circulating fluidized bed. *Powder Technol.* 2001;120:21–33.
21. Lim KS, Gururajan VS, Agarwal PK. Mixing of homogeneous solids in bubbling fluidized beds: theoretical modelling and experimental investigation using digital image analysis. *Chem Eng Sci.* 1993;48:2251–2265.
22. Holland DJ, Müller CR, Davidson JF, Dennis JS, Gladden LF, Hayhurst AN, Mantle MD, Sederman AJ. Time-of-flight variant to image mixing of granular media in a 3D fluidized bed. *J Magn Reson.* 2007;187:199–204.
23. Pallarès D, Johnsson H. A novel technique for particle tracking in cold 2-dimensional fluidized beds-simulating fuel dispersion. *Chem Eng Sci.* 2006;61:2710–2720.
24. Winaya INS, Shimizu T, Yamada D. A new method to evaluate horizontal solid dispersion in a bubbling fluidized bed. *Powder Technol.* 2007;178:173–178.
25. Mohs G, Gryczka O, Heinrich S, Mörl L. Magnetic monitoring of a single particle in a prismatic spouted bed. *Chem Eng Sci.* 2009;64:4811–4825.
26. Neri A, Gidaspow D. Riser hydrodynamics: simulation using kinetic theory. *AIChE J.* 2000;46:52–67.
27. Deen NG, Annaland MV, Van der Hoef MA, Kuipers JAM. Review of discrete particle modeling of fluidized beds. *Chem Eng Sci.* 2007;62:28–44.
28. Bokkers GA, van Sint Annaland M, Kuipers JAM. Mixing and segregation in a bidisperse gas-solid fluidised bed: a numerical and experimental study. *Powder Technol.* 2004;140:176–186.
29. Borodulya VA, Epanov YG, Teplitskii YS. Horizontal particle mixing in a free fluidized bed. *J Eng Phys Thermophys.* 1982;42:528–533.
30. Salam TF, Ren Y, Gibbs BM. Lateral solid and thermal dispersion in fluidized bed combustors. In: Proceedings of the 9th International Conference on FBC. Boston, MA: ASME. 1987:541–545.
31. Bi J, Yang G, Kojima T. Lateral mixing of coarse particles in fluidized-beds of fine particles. *Chem Eng Res Des.* 1995;73:162–167.

## Appendix

**Table A1. Complete Set of the Lateral Distribution of Tracer Mass Fraction**

| Row 1 | Row 2 | Row 3 | Row 4 | Row 1 | Row 2 | Row 3 | Row 4 | Row 1 | Row 2 | Row 3 | Row 4 |
|---|---|---|---|---|---|---|---|---|---|---|---|
| S1 | | | | M1-30 | | | | M3 | | | |
| 0.281 | 0.411 | 0.492 | 0.317 | 0.276 | 0.282 | 0.281 | 0.305 | 0.206 | 0.197 | 0.202 | 0.199 |
| 0.266 | 0.314 | 0.381 | 0.276 | 0.238 | 0.256 | 0.270 | 0.272 | 0.211 | 0.199 | 0.194 | 0.181 |
| 0.194 | 0.211 | 0.189 | 0.161 | 0.199 | 0.192 | 0.218 | 0.235 | 0.197 | 0.195 | 0.197 | 0.183 |
| 0.125 | 0.152 | 0.150 | 0.138 | 0.135 | 0.160 | 0.188 | 0.190 | 0.193 | 0.191 | 0.187 | 0.174 |
| 0.080 | 0.105 | 0.126 | 0.114 | 0.134 | 0.142 | 0.170 | 0.167 | 0.193 | 0.190 | 0.181 | 0.181 |
| 0.057 | 0.075 | 0.089 | 0.088 | 0.116 | 0.118 | 0.123 | 0.124 | 0.182 | 0.172 | 0.171 | 0.176 |
| S2 | | | | M2-5 | | | | M4 | | | |
| 0.201 | 0.212 | 0.208 | 0.202 | 0.314 | 0.308 | 0.319 | 0.318 | 0.182 | 0.182 | 0.188 | 0.182 |
| 0.202 | 0.202 | 0.201 | 0.194 | 0.277 | 0.286 | 0.267 | 0.257 | 0.180 | 0.195 | 0.185 | 0.185 |
| 0.193 | 0.203 | 0.197 | 0.191 | 0.229 | 0.207 | 0.194 | 0.218 | 0.176 | 0.174 | 0.179 | 0.182 |
| 0.181 | 0.200 | 0.198 | 0.181 | 0.155 | 0.194 | 0.154 | 0.162 | 0.180 | 0.166 | 0.179 | 0.180 |
| 0.169 | 0.175 | 0.178 | 0.189 | 0.093 | 0.114 | 0.114 | 0.112 | 0.172 | 0.178 | 0.166 | 0.163 |
| 0.160 | 0.172 | 0.167 | 0.180 | 0.072 | 0.079 | 0.079 | 0.075 | 0.167 | 0.166 | 0.163 | 0.171 |
| M1-5 | | | | M2-10 | | | | L1 | | | |
| 0.505 | 0.749 | 0.734 | 0.417 | 0.234 | 0.242 | 0.244 | 0.243 | 0.386 | 0.410 | 0.378 | 0.360 |
| 0.396 | 0.607 | 0.503 | 0.363 | 0.232 | 0.229 | 0.237 | 0.240 | 0.348 | 0.310 | 0.314 | 0.289 |
| 0.156 | 0.216 | 0.215 | 0.203 | 0.212 | 0.215 | 0.216 | 0.205 | 0.254 | 0.198 | 0.179 | 0.204 |
| 0.021 | 0.049 | 0.042 | 0.037 | 0.164 | 0.185 | 0.192 | 0.182 | 0.101 | 0.125 | 0.131 | 0.139 |
| 0.007 | 0.014 | 0.012 | 0.010 | 0.147 | 0.160 | 0.172 | 0.175 | 0.062 | 0.071 | 0.103 | 0.078 |
| 0.003 | 0.001 | 0.004 | 0.005 | 0.134 | 0.142 | 0.154 | 0.156 | 0.036 | 0.042 | 0.045 | 0.050 |
| M1-10 | | | | M2-15 | | | | L2 | | | |
| 0.380 | 0.704 | 0.666 | 0.418 | 0.202 | 0.200 | 0.196 | 0.198 | 0.281 | 0.289 | 0.294 | 0.322 |
| 0.334 | 0.562 | 0.502 | 0.350 | 0.184 | 0.195 | 0.182 | 0.177 | 0.252 | 0.252 | 0.271 | 0.263 |
| 0.150 | 0.211 | 0.203 | 0.182 | 0.183 | 0.188 | 0.186 | 0.172 | 0.199 | 0.220 | 0.245 | 0.217 |
| 0.067 | 0.069 | 0.073 | 0.097 | 0.175 | 0.185 | 0.177 | 0.173 | 0.148 | 0.178 | 0.193 | 0.166 |
| 0.026 | 0.030 | 0.034 | 0.049 | 0.158 | 0.181 | 0.168 | 0.157 | 0.103 | 0.122 | 0.148 | 0.144 |
| 0.013 | 0.016 | 0.012 | 0.013 | 0.146 | 0.161 | 0.154 | 0.155 | 0.092 | 0.093 | 0.101 | 0.098 |
| M1-15 | | | | M2-20 | | | | L3 | | | |
| 0.352 | 0.633 | 0.562 | 0.380 | 0.197 | 0.193 | 0.184 | 0.189 | 0.196 | 0.206 | 0.219 | 0.205 |
| 0.302 | 0.423 | 0.350 | 0.363 | 0.188 | 0.183 | 0.185 | 0.177 | 0.204 | 0.202 | 0.203 | 0.204 |
| 0.174 | 0.185 | 0.204 | 0.184 | 0.182 | 0.185 | 0.180 | 0.173 | 0.185 | 0.188 | 0.189 | 0.192 |
| 0.096 | 0.108 | 0.149 | 0.123 | 0.175 | 0.177 | 0.186 | 0.176 | 0.189 | 0.185 | 0.190 | 0.184 |
| 0.063 | 0.067 | 0.093 | 0.087 | 0.187 | 0.179 | 0.178 | 0.178 | 0.180 | 0.169 | 0.172 | 0.166 |
| 0.034 | 0.043 | 0.049 | 0.051 | 0.177 | 0.177 | 0.180 | 0.188 | 0.162 | 0.162 | 0.154 | 0.151 |
| M1-20 | | | | M2-30 | | | | L4 | | | |
| 0.345 | 0.485 | 0.408 | 0.336 | 0.175 | 0.181 | 0.184 | 0.191 | 0.193 | 0.193 | 0.191 | 0.189 |
| 0.277 | 0.317 | 0.296 | 0.324 | 0.186 | 0.187 | 0.191 | 0.186 | 0.198 | 0.201 | 0.200 | 0.202 |
| 0.163 | 0.186 | 0.208 | 0.224 | 0.180 | 0.185 | 0.183 | 0.173 | 0.180 | 0.189 | 0.186 | 0.175 |
| 0.152 | 0.148 | 0.172 | 0.155 | 0.183 | 0.187 | 0.188 | 0.170 | 0.181 | 0.197 | 0.179 | 0.180 |
| 0.115 | 0.102 | 0.108 | 0.106 | 0.186 | 0.189 | 0.186 | 0.178 | 0.188 | 0.176 | 0.169 | 0.167 |
| 0.117 | 0.071 | 0.077 | 0.081 | 0.175 | 0.175 | 0.176 | 0.184 | 0.174 | 0.169 | 0.156 | 0.165 |

*Manuscript received Sept. 5, 2009, and revision received July 2, 2010.*